Computer Physics Communications 219 (2017) 255–260

Contents lists available at ScienceDirect

Computer Physics Communications

journal homepage: www.elsevier.com/locate/cpc

A fast parallel 3D Poisson solver with longitudinal periodic and transverse open boundary conditions for space-charge simulations

Ji Qiang

Lawrence Berkeley National Laboratory, Berkeley, CA 94720, United States

ARTICLE INFO

Article history:
Received 8 November 2016
Received in revised form 29 May 2017
Accepted 5 June 2017
Available online 27 June 2017

Keywords:
Poisson solver
Spectral finite-difference method
Periodic and open boundary conditions

ABSTRACT

A three-dimensional (3D) Poisson solver with longitudinal periodic and transverse open boundary conditions can have important applications in beam physics of particle accelerators. In this paper, we present a fast efficient method to solve the Poisson equation using a spectral finite-difference method. This method uses a computational domain that contains the charged particle beam only and has a computational complexity of $O(N_u(logN_{mode}))$, where N_u is the total number of unknowns and N_{mode} is the maximum number of longitudinal or azimuthal modes. This saves both the computational time and the memory usage of using an artificial boundary condition in a large extended computational domain. The new 3D Poisson solver is parallelized using a message passing interface (MPI) on multi-processor computers and shows a reasonable parallel performance up to hundreds of processor cores.

1. Introduction

The particle accelerator as one of the most important inventions of the twenty century has many applications in science and industry. In accelerators, a train of charged particle (e.g. proton or electron) beam bunches are transported and accelerated to high energy for different applications. To study the dynamics of those charged particles self-consistently inside the accelerator, the particle-in-cell (PIC) model is usually employed in simulation codes (e.g. the WARP and the IMPACT code suite [1–3]). This PIC model includes both the space-charge forces from the Coulomb interactions among the charged particles within the bunch and the forces from external accelerating and focusing fields at each time step. To calculate the space-charge forces, one needs to solve the Poisson equation for a given charge density distribution. A key issue in the PIC simulation is to solve the Poisson equation efficiently, at each time step, subject to appropriate boundary conditions.

Solving the 3D Poisson equation for the electric potential of a charged beam bunch with longitudinal periodic and transverse open boundary conditions can have important applications in beam dynamics study of particle accelerators. In the accelerator, a train of charged particle bunches as shown in Fig. 1 are produced, accelerated, and transported. If the separation between two bunches is large, each bunch can be treated as an isolated bunch, and the 3D open boundary conditions can be used to solve the Poisson equation. In some accelerators such as a Radio-Frequency Quadrupole (RFQ), the separation between particle bunches is short, to model a single bunch, one needs to use the longitudinal periodic boundary condition [4]. The same model can be used to study space-charge effects in a longitudinally modulated electron beam, where the electron beam density varies periodically from the interaction with the laser beam and the magnetic optic elements [5].

In previous studies, a number of methods for solving 3D Poisson's equation subject to a variety of boundary conditions have been studied [6–21]. However, none of these methods handles the Poisson equation with the longitudinal periodic and transverse open boundary conditions. In the code of Ref. [2], an image charge method is used to add the contributions from longitudinally periodic bunches into the single bunch's Green function. Then an FFT method is used to effectively calculate the discrete convolution between the charge density and the new Green's function that includes contributions from other bunches. The computational cost of this method scales as $O(Nlog(N))$. However, this method requires the computation of the Green's function from multiple bunch summation. It is not clear, how many bunches are needed in order to accurately emulate the longitudinal periodic boundary condition. In Ref. [5], the image charge method is used with special function to approximate the summation of the Green's function in different regimes. In practical application, one may not know beforehand what regime should be used for a good approximation. Besides the complexity of the new Green's function in the image charge method, to use the FFT to calculate the discrete convolution, one needs to double the computational domain with zero padding [8,22]. This increases both the computational time and the memory usage.

E-mail address: JQiang@lbl.gov.

http://dx.doi.org/10.1016/j.cpc.2017.06.002
0010-4655/© 2017 Elsevier B.V. All rights reserved.

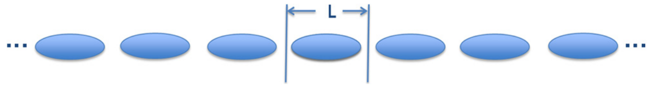

Fig. 1. A schematic plot of a train of charged particle beam bunches in the particle accelerator.

In this paper, we propose a fast efficient method to solve the 3D Poisson equation with the longitudinal periodic and transverse open boundary conditions. We use a Galerkin spectral Fourier method to approximate the electric potential and the charge density function in the longitudinal and azimuthal dimensions where periodic boundary conditions are satisfied. We then use a second order finite-difference method to solve the radial ordinary differential equation for each mode subject to the transverse open boundary condition. Instead of using a large radial domain with empty space and artificial finite Dirichlet boundary condition to approximate the open boundary condition, we use a domain that contains only the charged particle beam and a boundary matching condition to close the group of linear algebraic equations for each mode. This group of tridiagonal linear algebraic equations can be solved efficiently using the direct Gaussian elimination with a computational cost $O(N)$, where N is the number of unknowns on the radial grid.

The organization of this paper is as follows: After the introduction, we describe the proposed spectral finite-difference numerical method in Section 2. Several numerical tests of the new algorithm and a comparison with the artificial boundary condition are presented in Section 3. The parallel implementation of the new 3D Poisson solver on multi-processor computer is presented in Section 4. The conclusions are drawn in Section 5.

2. The spectral finite-difference method

The three dimensional Poisson equation in cylindric coordinates can be written as:

$$\frac{\partial^2\phi}{\partial r^2}+\frac{1}{r}\frac{\partial\phi}{\partial r}+\frac{1}{r^2}\frac{\partial^2\phi}{\partial\theta^2}+\frac{\partial^2\phi}{\partial z^2}=-\rho(r,\theta,z) \tag{1}$$

where ϕ denotes the electric potential, ρ the charge density function, r and z the radial and longitudinal distance. The longitudinal periodic and transverse open boundary conditions for the potential are:

$$\phi(r=\infty,\theta,z)=0 \tag{2}$$

$$\phi(r,\theta+2\pi,z)=\phi(r,\theta,z) \tag{3}$$

$$\phi(r,\theta,z+L)=\phi(r,\theta,z). \tag{4}$$

Given the periodic boundary conditions of the electric potential along the θ and the z, we use a Galerkin spectral method with the Fourier basis function to approximate the charge density function ρ and the electric potential ϕ along these two dimensions as:

$$\rho(r,\theta,z)=\sum_{n=-N_n/2}^{n=N_n/2-1}\sum_{m=-N_m/2}^{m=N_m/2-1}\rho_n^m(r)\exp(-ia_nz)\exp(-im\theta) \tag{5}$$

$$\phi(r,\theta,z)=\sum_{n=-N_n/2}^{n=N_n/2-1}\sum_{m=-N_m/2}^{m=N_m/2-1}\phi_n^m(r)\exp(-ia_nz)\exp(-im\theta) \tag{6}$$

where

$$\rho_n^m(r)=\frac{2}{L\pi}\int_0^L\int_0^{2\pi}\rho(r,\theta,z)\exp(im\theta)\exp(ia_nz)\,d\theta dz \tag{7}$$

$$\phi_n^m(r)=\frac{2}{L\pi}\int_0^L\int_0^{2\pi}\phi(r,\theta,z)\exp(im\theta)\exp(ia_nz)\,d\theta dz \tag{8}$$

and $a_n=n2\pi/L$, L is the longitudinal periodic length. Substituting the above expansions into the Poisson equation (1) and making use of the orthonormal condition of the Fourier function, we obtain:

$$\frac{\partial^2\phi_n^m}{\partial r^2}+\frac{1}{r}\frac{\partial\phi_n^m}{\partial r}-\left(\frac{m^2}{r^2}+(a_n)^2\right)\phi_n^m=-\rho_n^m. \tag{9}$$

This is a group of decoupled ordinary differential equations that can be solved for each individual mode m and n. For these equations, at $r=0$, we have the boundary conditions:

$$\frac{\partial\phi_n^m}{\partial r}(0)=0;\ \ for\ \ m=0 \tag{10}$$

$$\phi_n^m(0)=0;\ \ for\ \ m\neq0. \tag{11}$$

Assuming all charged particles within the beam bunch are contained within a radius R, we discretize the above equation using a second order finite-difference scheme, and obtain a group of linear algebraic equations for each mode (m,n) as:

$$\left(\frac{r_i^2}{h^2}-\frac{r_i}{2h}\right)\phi_n^m(r_{i-1})-\left(\frac{2r_i^2}{h^2}+m^2+a_n^2r_i^2\right)\phi_n^m(r_i)+\left(\frac{r_i^2}{h^2}+\frac{r_i}{2h}\right)\phi_n^m(r_{i+1})=-r_i^2\rho_n^m(r_i) \tag{12}$$

where $i=1,2,\ldots,N$, and $r_i=ih$. The boundary conditions at $r=0$ are approximated as:

$$-\frac{3}{2}\phi_n^m(r_0)+2\phi_n^m(r_1)-\frac{1}{2}\phi_n^m(r_2)=0;\ \ for\ \ m=0 \tag{13}$$

$$\phi_n^m(r_0)=0;\ \ for\ \ m\neq0. \tag{14}$$

For $m=0$, there are only $N+1$ linear equations but $N+2$ unknowns, and for $m\neq0$, there are only N linear equations but $N+1$ unknowns. For the potential outside the radius R, Eq. (9) can be written as:

$$\frac{\partial^2\phi_n^m}{\partial r^2}+\frac{1}{r}\frac{\partial\phi_n^m}{\partial r}-\left(\frac{m^2}{r^2}+(a_n)^2\right)\phi_n^m=0 \tag{15}$$

subject to the open boundary conditions

$$\phi_n^m(r=\infty)=0. \tag{16}$$

For $n\neq0$, a formal solution of Eq. (15) subject to the boundary condition (16) can be written as:

$$\phi_n^m(r)=A\,K_m(a_nr), \tag{17}$$

where K_m is the second kind modified Bessel function. Using the above equation and the continuity of the potential at r_N, we obtain another equation for the unknowns $\phi_n^m(r_N)$ and $\phi_n^m(r_{N+1})$ as:

$$\phi_n^m(r_N)K_m(a_nr_{N+1})=\phi_n^m(r_{N+1})K_m(a_nr_N). \tag{18}$$

For $n=0,m\neq0$, Eq. (15) is reduced to the Cauchy–Euler equation:

$$\frac{\partial^2\phi_0^m}{\partial r^2}+\frac{1}{r}\frac{\partial\phi_0^m}{\partial r}-\frac{m^2}{r^2}\phi_0^m=0. \tag{19}$$

A formal solution of this equation that satisfies the open radial boundary condition can be written as:

$$\phi_0^m(r)=Ar^{-m}. \tag{20}$$

From the above equation, we obtain another equation for the unknowns $\phi_0^m(r_N)$ and $\phi_0^m(r_{N+1})$ as:

$$\phi_0^m(r_N)r_N^m=\phi_0^m(r_{N+1})r_{N+1}^m. \tag{21}$$

For $n=0$, $m=0$, Eq. (15) is reduced to:

$$\frac{\partial^2\phi_0^0}{\partial r^2}+\frac{1}{r}\frac{\partial\phi_0^0}{\partial r}=0. \tag{22}$$

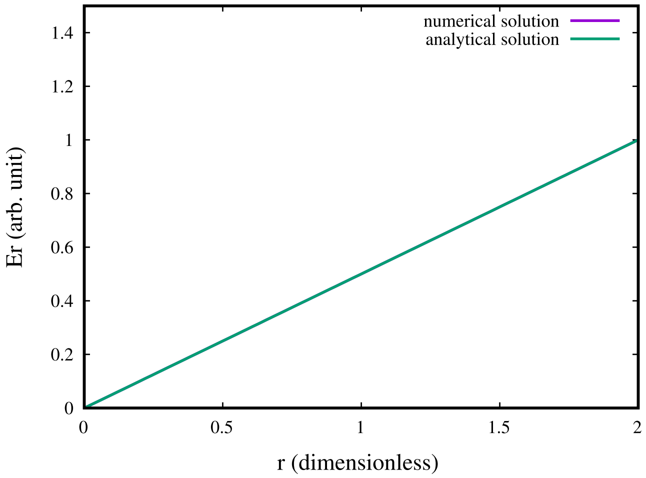

Fig. 2. Transverse radial electric field profile Er in the middle of the bunch from the numerical solution together with the analytical solution in a uniform cylinder coasting beam. Here two solutions overlie each other.

A formal solution of this equation that satisfies the open radial boundary condition can be written as:

$$\phi_0^0(r) = A\log(r). \tag{23}$$

From this equation, we obtain another equation for the unknowns $\phi_0^0(r_N)$ and $\phi_0^0(r_{N+1})$ as:

$$\phi_0^0(r_N)\log(r_{N+1}) = \phi_0^0(r_{N+1})\log(r_N). \tag{24}$$

Using Eqs. (18), (21) and (24), we have $N+2$ linear equations for $N+2$ unknowns for $m = 0$ and $N+1$ linear equations for $N+1$ unknowns for $m \neq 0$. For each mode m and n, this is a group of tridiagonal linear algebraic equations, which can be solved effectively using direct Gaussian elimination with the number of operations scaling as $O(N)$. Since both Fourier expansions in θ and z can be computed very effectively using the FFT method, the total computational complexity of the proposed algorithm scales as $O(NN_mN_n log(N_mN_n))$.

3. Numerical tests

The numerical algorithm discussed in the preceding section is tested using two charge density distribution functions. The first example is an infinite long cylindric coasting beam with uniform charge distribution within the radius $R = 2$. The charge density function is given as

$$\rho(r,\theta,z) = \begin{cases} 1.0 : r \le 2 \\ 0.0 : r > 2. \end{cases} \tag{25}$$

For this charge density function, there is only the radial component of the electric field. The analytical solution of the electric field can be found as:

$$E_r(r) = \frac{r}{2} \; for \; r \le 2. \tag{26}$$

Fig. 2 shows the transverse radial electric field from the numerical solution and the above analytical solution. It is seen that the numerical solution agrees with the analytical solution very well. Actually, these two solutions are nearly identical to each other (except the origin point with 10^{-15} difference). This is due to the fact that the solver has second-order accuracy in radial direction and can approximate the quadratic function exactly, which is true for this test example with constant source term.

In the second test example, we assume that there is a longitudinal modulation of the charged particle density distribution. The charge density function is given as:

$$\rho(r,\theta,z) = \begin{cases} 4 - 4(r/R)^2 + \sin(a_1 z)[4-(a_1 r)^2]/5 : r \le R \\ 0.0 : r > R. \end{cases} \tag{27}$$

The analytical solution of the electric fields for this charge distribution can be written as:

$$E_z(r,z) = a_1\cos(a_1 z)[r^2 - AI_0(a_1 r)]/5 \tag{28}$$

$$E_r(r,z) = 2r - r^3/R^2 + \sin(a_1 z)[2r - Aa_1 I_1(a_1 r)]/5 \tag{29}$$

where the constant A is given as:

$$A = \frac{R^2 a_1 K_1(a_1 R) + 2RK_0(a_1 R)}{a_1 I_1(a_1 R)K_0(a_1 R) + a_1 I_0(a_1 R)K_1(a_1 R)}. \tag{30}$$

Here, the matching condition at the edge R is used together with the analytical formal solution Eq. (17) for the open boundary condition to determine the above constant A. Figs. 3 and 4 show the longitudinal electric field and the transverse radial electrical field from the numerical solutions and from the analytical solutions. Here, the relative errors of the fields are computed from the differences of the numerical solution and the analytical solution normalized by the maximum value of the analytical solution. The numerical solutions and the analytical solutions agree with each other very well in this longitudinally modulated charged particle beam too. Here, we have assumed $R = 10$ and $L = \pi R$.

The numerical method proposed in the preceding section has the advantage that uses a computational domain that contains the charged particle beam only while satisfying the transverse open boundary condition. In principle, the transverse open boundary can be approximated by an artificial closed Dirichlet boundary condition in a larger computational domain. Since only the electric fields inside the charge particle beam bunch are needed in the self-consistent accelerator space-charge beam dynamics simulation, this larger computational domain by using the artificial Dirichlet boundary condition will waste both the computational time and the memory storage in the empty computational domain. In the following, we use a simplified one-dimensional equation from above equations to illustrate the advantage of the above proposed method.

For $m = 0$ and $n = 1$, Eq. (9) is reduced to:

$$\frac{\partial^2\phi_1^0}{\partial r^2} + \frac{1}{r}\frac{\partial\phi_1^0}{\partial r} - a_1^2\phi_1^0 = -\rho_1^0. \tag{31}$$

Assuming a radial charge distribution $\rho_1^0(r)$ as:

$$\rho_1^0(r) = \begin{cases} 4-(a_1 r)^2 : r \le R \\ 0.0 : r > R \end{cases} \tag{32}$$

we can have an analytical solution as:

$$\phi_1^0(r) = -r^2 + AI_0(a_1 r) \tag{33}$$

where the constant A is given in Eq. (30). Fig. 5 shows the electric potential and the relative errors as a function of radial distance from the analytical solution, and from the proposed numerical solution with transverse open boundary condition ($R = 10$), from the artificial transverse closed Dirichlet boundary condition using two times computational domain ($\phi_1^0(R = 20) = 0$), and from the artificial transverse closed boundary condition using four times computational domain ($\phi_1^0(R = 40) = 0$). It is seen that even using two times computational domain, the artificial closed boundary condition solution still shows much larger errors than the proposed open boundary numerical solution. It appears that four times larger computational domain is needed in the artificial closed boundary solution in order to attain the same numerical accuracy

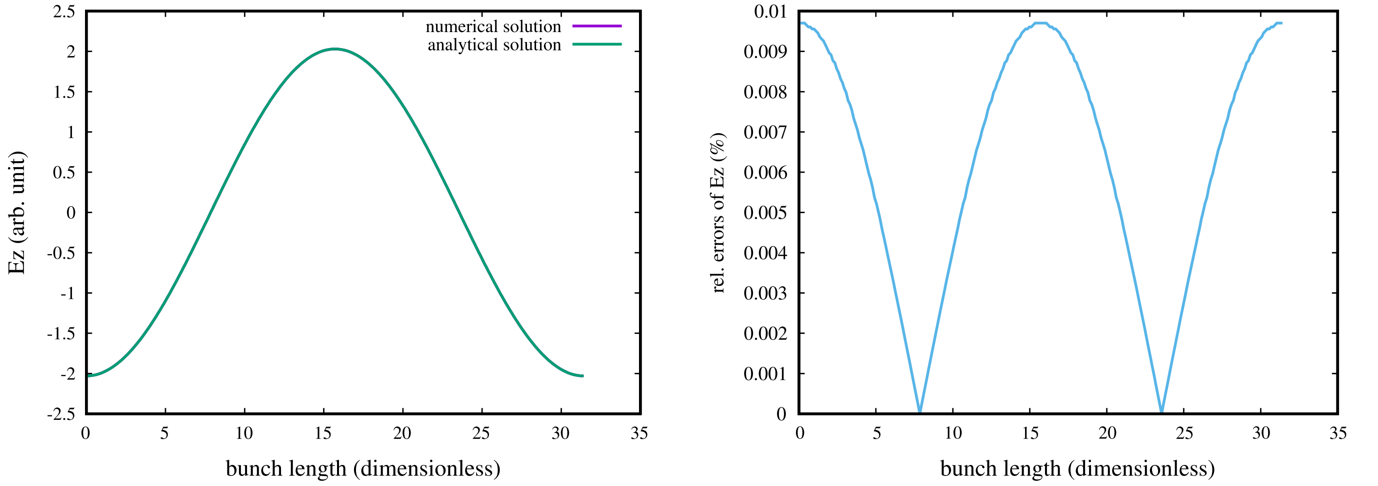

Fig. 3. Longitudinal electric field profile E_z on the z-axis from the numerical solutions together with the analytical solutions (left) and the relative errors of the E_z (right) in a longitudinally modulated charged particle beam bunch.

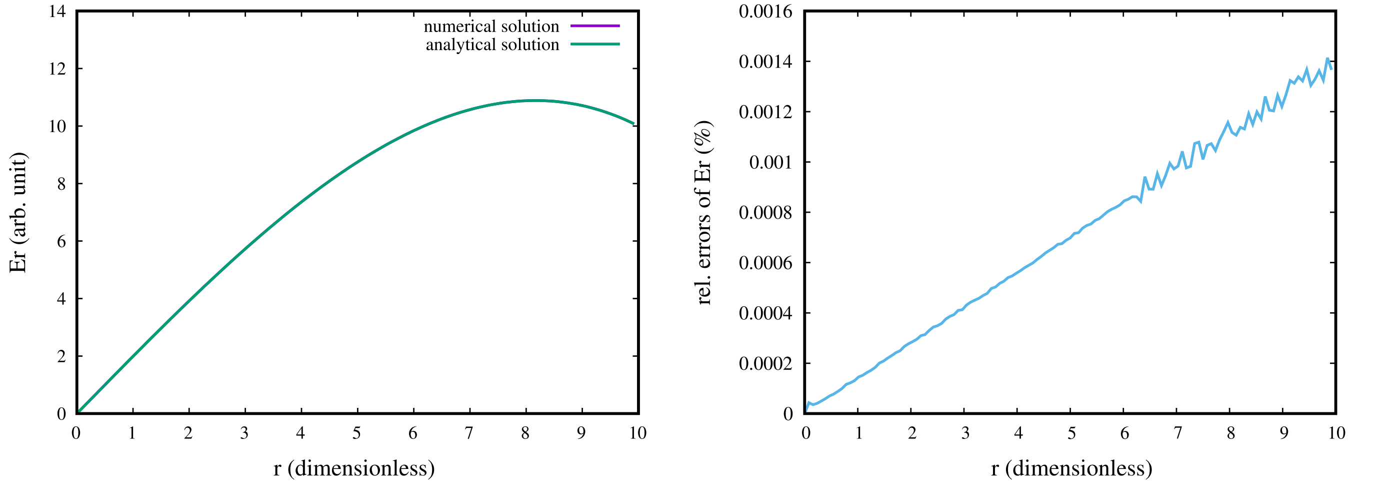

Fig. 4. Transverse radial electric field profile E_r in the middle of the bunch from the numerical solutions together with the analytical solutions (left) and the relative errors of the E_r (right) in a longitudinally modulated charged particle beam bunch.

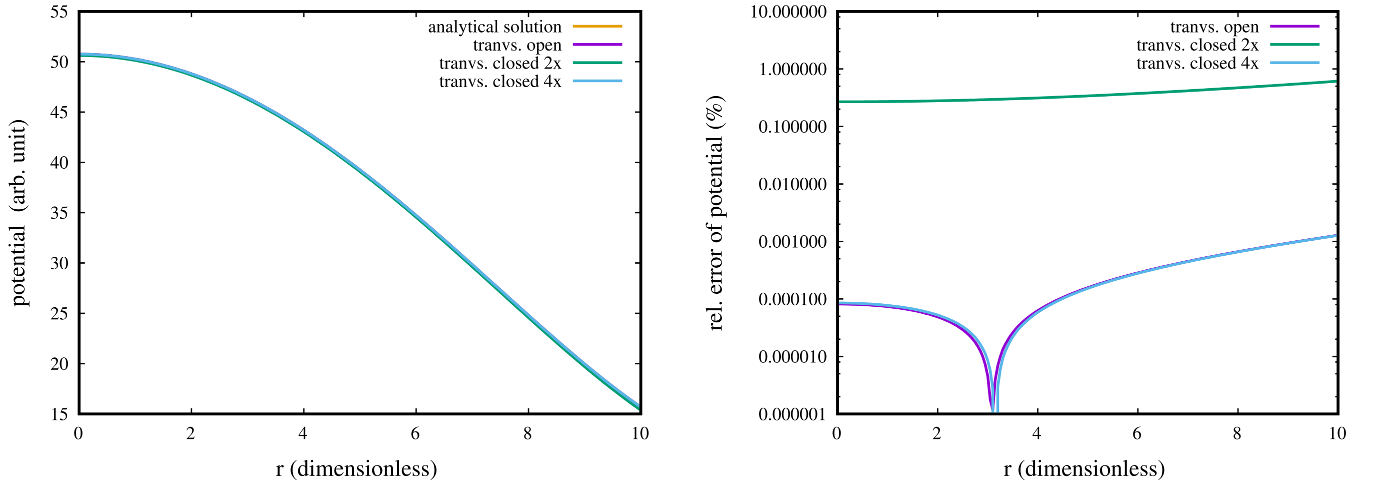

Fig. 5. The electric potential (left) and the relative errors (right) from the analytical solution and from the numerical solution with transverse open, transverse closed with two times radial computational domain, and transverse closed with four times computational domain.

as the open boundary solution that uses a domain with radius R that contains the charged particle beam only. In the above example, we have used 201 radial grid points for the open boundary solution, 401 grid points for the artificial closed boundary solution with two times computational domain and 801 grid points for the solution with four times computational domain.

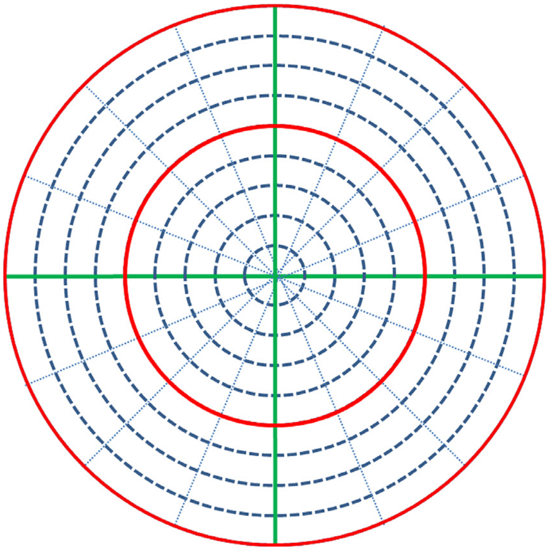

Fig. 6. A schematic plot of the two-dimensional domain-decomposition in the r–θ dimension with a serial z dimension pointing into the paper. (For interpretation of the references to colour in this figure legend, the reader is referred to the web version of this article.)

4. Parallel implementation

The numerical algorithm proposed in Section 2 was implemented on multi-processor parallel computers. A two-dimensional domain-decomposition method was employed to implement the above algorithm. A schematic plot of the two-dimensional domain-decomposition of the computational domain in the $r-\theta$ dimension with a serial dimension in the z direction is given in Fig. 6. Here, the dashed lines are computational grids along the radial r and the azimuthal θ dimensions. The solid lines (red and green) denote the two-dimensional logical processor layout with two processors along r dimension and four processors along the θ dimension (total eight processors). Each processor contains a sector of dashed line grid points as shown in the figure. The number of grid points on each processor is kept as equal as possible by uniformly dividing numerical grid points among the number of processors in each dimension in order to attain a good load balance.

After mapping the computational domain onto processors, the solution of the Poisson equation using above algorithm can be done on each processor. Since each processor contains all the grid points along the z dimension, the Fourier expansion along this direction using the FFT can be done simultaneously on all processors. After the FFT in z dimension, a parallel transpose is employed to switch the distributed θ component with the serial z component so that each processor contains all the grid points along the θ dimension after the transpose. Then the Fourier expansion along the θ dimension can be done simultaneously on all processors using the FFT. After the Fourier expansion in θ dimension, a second transpose is used to switch the distributed radial component with the serial θ component so that each processor contains all radial grid points. The fast Gaussian elimination following above algorithm is done for each mode (m, n) simultaneously on all processors. After the solution of radial dependent equation for each mode, another transpose is used to switch the radial component with the θ component and followed by an inverse FFT in the θ dimension on each processor simultaneously. Then another transpose is used to switch the θ component and the z component, and followed by an inverse FFT in the z dimension. The parallel transpose used to switch the distributed component into the serial component involves global communication among all processors using the MPI.

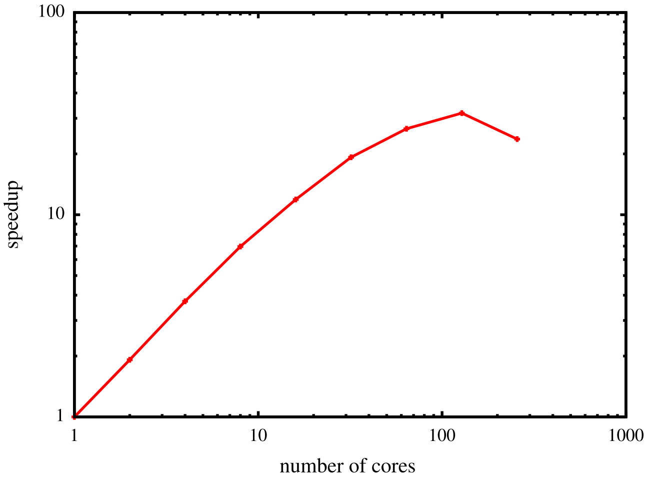

Fig. 7. The speedup of the parallel Poisson solver as a function of the number of cores on a Cray XC30 supercomputer.

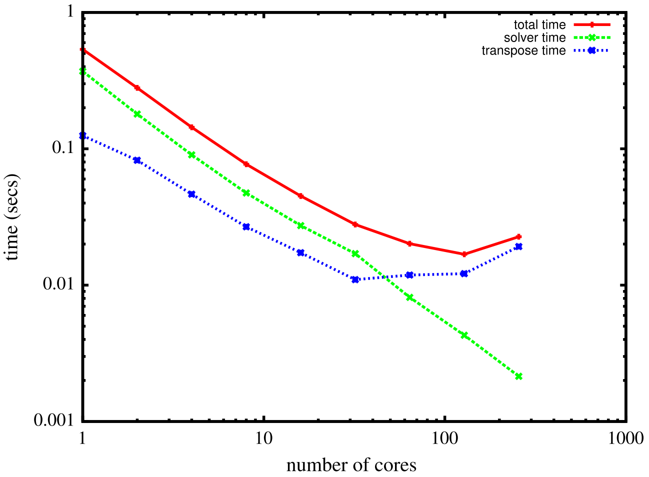

Fig. 8. The total computing time (red), the direct numerical solver time (green), and the parallel transpose time (blue) as a function of the number of cores on a Cray XC30 supercomputer. (For interpretation of the references to colour in this figure legend, the reader is referred to the web version of this article.)

The performance of the parallel Poisson solver was tested on a Cray XC30 supercomputer located at the National Energy Research Scientific Computing center [23]. This computer is a distributed share memory parallel computer that has more than five thousand nodes and each node contains two sockets, each with 12-core Intel "Ivy Bridge" processor. Fig. 7 shows the speedup of the solver on this computer for a problem size of 256 ×128 ×128, each corresponding to r, θ, and z direction. It is seen that the parallel solver has good scalability up to hundred processors for this problem size. Fig. 8 shows the total time, the time used in direct numerical solution (the FFTs and the Gaussian elimination), and time used in the parallel transpose as a function of the number of cores for above test example. The direct numerical solver time goes down almost linearly with the increase of the number of cores. The parallel transpose time decreases linearly within a small number of cores and starts to increase beyond 32 cores due to the global communication among all processors. This limits the total scalability of the parallel Poisson solver on large scale supercomputers.

5. Conclusions and discussions

In this paper, we presented a fast three-dimensional parallel Poisson solver subject to the longitudinal periodic and transverse open boundary conditions. Instead of using an enlarged artificial computational domain with closed Dirichlet boundary condition, this solver uses a computational domain that contains the charged particles source term only. This saves both the computational time and the memory usage compared with the artificial closed boundary condition method. By using the FFT method to calculate the longitudinal and azimuthal Fourier expansion and the direct Gaussian elimination to solve the radial tridiagonal linear algebraic equations, the computational complexity of the proposed numerical method scales as $O(N_u(\log N_{mode}))$. The new 3D Poisson solver is also parallelized using a message passing interface (MPI) on multi-processor computers and has a good parallel speedup up to hundreds of processors. This fast parallel Poisson solver can be included in the self-consistent PIC codes for space-charge beam physics study in particle accelerators.

The Poisson solver proposed in this paper uses a cylindrical coordinate system. This coordinate system works especially well for a transverse round or nearly round charged particle beam since only one or a few Fourier modes are needed to represent the azimuthal density variation. For a beam with large transverse aspect ratio, it may need a large number of modes to represent the transverse density distribution. The exact number of Fourier modes needed to represent the charge density distribution depends on the physical applications. For a smooth function, the spectral approximation has an accuracy whose numerical error scales as $\exp(-cN)$ with $c > 0$ and N the number of modes in the approximation [24]. The accuracy of the proposed Poisson solver scales as $O(h^2 + exp(-cN))$, where h is the radial grid size, and is independent of the longitudinal-to-transverse aspect ratio. To further improve numerical accuracy of the solver, it will be useful to extend the second-order finite-difference scheme in radial direction to higher order scheme, e.g. using a discretization in Ref. [25]. Such an extension will be reported in our future study.

Acknowledgments

This work was supported by the U.S. Department of Energy under Contract No. DE-AC02-05CH11231. This research used computer resources at the National Energy Research Scientific Computing Center.

References

[1] A. Friedman, D.P. Grote, I. Haber, Phys. Fluids B 4 (7) (1992) 2203–2210.
[2] J. Qiang, R.D. Ryne, S. Habib, V. Decyk, J. Comput. Phys. (ISSN: 0021-9991) 163 (2) (2000) 434–451. http://dx.doi.org/10.1006/jcph.2000.6570. http://www.sciencedirect.com/science/article/pii/S0021999100965707.
[3] J. Qiang, S. Lidia, R.D. Ryne, C. Limborg-Deprey, Phys. Rev. ST Accel. Beams 9 (2006) 044204.
[4] R. Duperrier, Phys. Rev. ST Accel. Beams 3 (2000) 124201.
[5] M. Dohlus, Ch. Henning, Phys. Rev. ST Accel. Beams 19 (2016) 034401.
[6] D.B. Haidvogel, T. Zang, J. Comput. Phys. 30 (1979) 167.
[7] S. Ohring, J. Comput. Phys. 50 (1983) 307.
[8] R.W. Hockney, J.W. Eastwood, Computer Simulation Using Particles, Adam Hilger, New York, 1988.
[9] H. Dang-Vu, C. Delcarte, J. Comput. Phys. 104 (1993) 221.
[10] E. Braverman, M. Israeli, A. Averbuch, L. Vozovoi, J. Comput. Phys. 144 (1998) 109.
[11] L. Plagne, J. Berthou, J. Comput. Phys. 157 (2000) 419.
[12] J. Qiang, R.D. Ryne, Comput. Phys. Comm. 138 (2001) 18.
[13] J. Qiang, R. Gluckstern, Comput. Phys. Comm. 160 (2004) 120.
[14] M. Lai, Z. Li, X. Lin, J. Comput. Appl. Math. 191 (2006) 106.
[15] P. McCorquodale, P. Colella, G.T. Balls, S.B. Baden, Commun. Appl. Math. Comput. Sci. 2 (2007) 57.
[16] J. Xu, P.N. Ostroumov, J. Nolen, Comput. Phys. Comm. 178 (2008) 290.
[17] R.D. Ryne, arXiv:1111.4971v1, 2011.
[18] M.M. Hejlesen, J.T. Rasmussen, P. Chatelain, J.H. Walther, J. Comput. Phys. 252 (2013) 458.
[19] D. Zheng, G. Poplau, U. van Rienen, Comput. Phys. Comm. 198 (2016) 82.
[20] J. Qiang, Comput. Phys. Comm. 203 (2016) 122.
[21] C.R. Anderson, J. Comput. Phys. 314 (2016) 194.
[22] W.H Press, B.P. Flannery, S.A. Teukolsky, W.T. Vetterling, Numerical Recipes in FORTRAN: The Art of Scientific Computing, second ed., Cambridge University Press, Cambridge, England, 1992.
[23] http://www.nersc.gov/users/computational-systems/edison/configuration/.
[24] D. Gottlieb, S.A. Orszag, Numerical Analysis of Spectral Methods: Theory and Applications, Society for Industrial and Applied Mathematics, 1977.
[25] C.R. Anderson, Uniform Grid Computation of Smooth Hydrogenic Orbitals, UCLA CAM Report 15-09, 2015.